

pubs.acs.org/JACS Article

Synergy between Photoluminescence and Charge Transport Achieved by Finely Tuning Polymeric Backbones for Efficient Light-Emitting Transistor

Dafei Yuan, Mohammad A. Awais, Valerii Sharapov, Xunshan Liu, Andriy Neshchadin, Wei Chen, and Luping Yu*



Cite This: J. Am. Chem. Soc. 2021, 143, 5239-5246



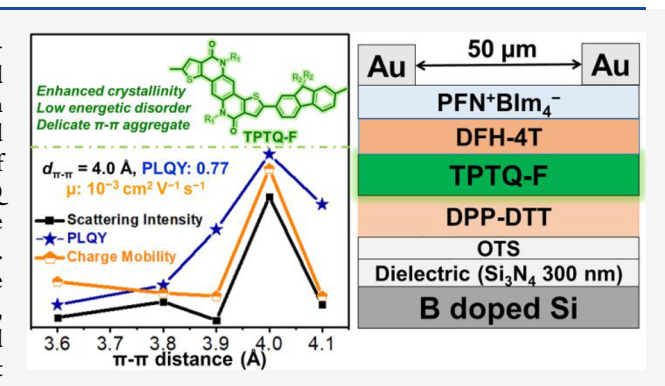
ACCESS

Metrics & More

Article Recommendations

Supporting Information

ABSTRACT: The lack of design principle for developing high-performance polymer materials displaying strong fluorescence and high ambipolar charge mobilities limited their performance in organic light-emitting transistors (OLETs), electrically pumped organic laser, and other advanced electronic devices. A series of semiladder polymers by copolymerization of weak acceptors (TPTQ or TPTI) and weak donors (fluorene (F) or carbazole (C)) have been developed for luminescent and charge transporting properties. It was found that enhanced planarity, high crystallinity, and a delicate balance in interchain aggregation obtained in the new copolymer, TPTQ-F, contributed to high ambipolar charge mobilities and photoluminescent quantum yield. TPTQ-F showed excellent performance in solution-processed multilayered OLET devices with an external quantum efficiency (EQE) of 5.3%.



INTRODUCTION

The unique photophysical properties of organic conjugated polymers have been explored for electrical and optical devices with performances comparable to traditionally silicon-based semiconductors. These polymers are solution-processable, enabling spin-coating, roll-to-roll processing, or inkjet-printing in manufacturing. The resulting devices can also be flexible and stretchable, ideal to prepare wearable electronic and bioelectronic devices. The most successful applications of these materials (both polymers and small conjugated molecules) are in the development of organic light-emitting diodes (OLEDs), creating a big impact in optical display. 6,7

Organic light-emitting transistors (OLETs) combine the advantages of logic function of organic field-effect transistors (OFETs) and electroluminescent properties of OLEDs into a single device. Therefore, OLETs provide a unique platform to simultaneously investigate charge transporting and electroluminescent behaviors. OLETs can also be used in simplified optical displays, electrically pumped organic laser, and so on. An OLET material required not only high and balanced ambipolar FET charge mobilities but also high photoluminescent quantum yield (PLQY).

Though small-molecule based OLETs have recently achieved high external quantum efficiency (EQE) and electroluminescent intensity, ^{22–28} polymer-based OLETs are lagging behind. ^{29–34} To achieve high-performance small-molecule OLETs, one must consider the control of

intermolecular interaction, the crystal structure, and grain boundary of crystalline to balance the charge transport and fluorescence.^{35–38} For polymeric OLET materials, both the interchain and intrachain interactions should be considered.^{2,39-42} One must design polymer structures with high fluorescent and semiconductive properties in solid state. Good solubility in common solvents is crucial, which requires suitable alkyl side chains attached to the conjugated backbone. Equally important is to balance high charge mobilities and PLQY via control in the interchain $\pi - \pi$ stacking distances.^{43,44} Moreover, the degree of energetic disorder and conformations in polymer chains will significantly influence the PLQY in solution and solid states. 45 To achieve balanced electron and hole injections, matched energy levels between OLET materials and electrodes are prerequisite. The highest occupied molecular orbital (HOMO) and the lowest unoccupied molecular orbital (LUMO) energy levels are ideal when close to the work-function (WF) of metal electrodes. It is important to realize that it remains a great challenge to

Received: February 10, 2021 Published: March 23, 2021





integrate all these desired properties in a single polymer system.

We have synthesized a series of semiladder copolymers, TPTI-CC, TPTI-F, TPTQ-C, and TPTQF-C (Figure 1a,b), by

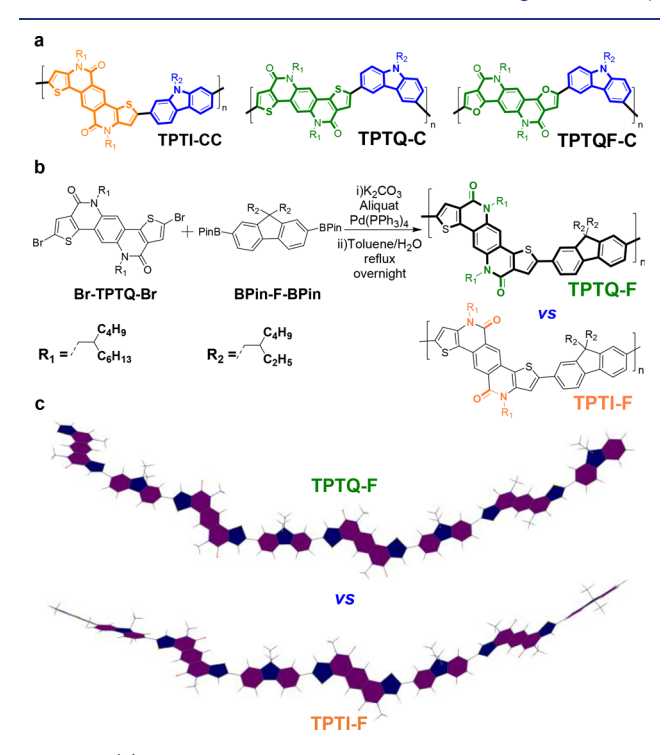


Figure 1. (a) Chemical structures of previously developed semiladder type copolymers TPTI-CC, TPTQ-C, and TPTQF-C in our groups. (b) Synthesis of semiladder type copolymer TPTQ-F and the chemical structure of TPTI-F. (c) Optimized molecular structures of the two semiladder polymers (top, TPTQ-F; bottom, TPTI-F) using DFT calculation (four repeating units, B3LYP method, 6-31g** basis set).

copolymerization of weak acceptor monomer 4,10-bis(2-butyloctyl)thieno[2',3':5,6]pyrido[3,4-g]thieno[3,2-c]-isoquinoline-5,11-dione (TPTI) or 5,11-bis(2-butyloctyl)-thieno[2',3':4,5]pyrido[2,3-g]thieno[3,2-c]quinoline-4,10-dione (TPTQ) and weak donor monomer carbazole (C) or fluorene (F). Among them, TPTI-F showed the highest PLQY (Table S1) and impressive EQE (2.8%) in multilayered OLET devices. However, theoretical calculation and experiments indicated that TPTI-F exhibited highly twisted polymer backbones, interchain H-aggregates, and amorphous microstructures. Though its PLQY of 59% was relatively high, only unipolar charge mobility as low as 10^{-6} cm² V⁻¹ s⁻¹ and small $I_{\rm on/off}$ of 10^{1} were achieved in single-layered FET devices due to the poor planarity and weak crystallinity.

To optimize both the PLQY and FET properties, we synthesized a new semiladder copolymer TPTQ-F. The TPTQ ladder structure exhibits a highly planar backbone and larger

electron affinity in comparison with TPTI, ^{48,49} which will contribute to more ordered intermolecular stacking and lower LUMO energy levels in TPTQ-F. Indeed, TPTQ-F exhibited enhanced planarity, deeper LUMO energy levels, interchain Jaggregates, and high crystallinity with face-on orientation. Moreover, the delicate balance in interchain π – π distance (4.0 Å) contributes to a high PLQY of 77% and ambipolar charge mobilities of 1.26×10^{-3} cm² V⁻¹ s⁻¹ and 3.53×10^{-4} cm² V⁻¹ s⁻¹ for hole and electron, respectively. These improvements lead to multilayered OLET devices with an EQE of 5.3% and EL intensity of 414 nW.

RESULTS AND DISCUSSION

The TPTQ dibromide (Br-TPTQ-Br) monomer and fluorene (F) monomer containing bis(pinacolato)diboron (BPin) moieties (BPin-F-BPin) were synthesized according to the reported procedure. 46,49 The semiladder copolymer, TPTQ-F, was synthesized via Suzuki-coupling polymerization as shown in Figure 1b. The yellow-green solid of TPTQ-F was obtained in a yield of 80% after Soxhlet extraction and reprecipitation of the chloroform fraction in methanol. The characterization by ¹H nuclear magnetic resonance (NMR) and elemental analysis for TPTQ-F, as summarized in Supporting Information, supported the structure as proposed. TPTQ-F exhibited moderate molecular weights ($M_{\rm w} = 55\,172$; $M_{\rm n} = 36\,012$) and narrow polydispersity indices (PDI) of 1.53 (Table 1). Thermogravimetric analysis (TGA) showed high thermal stability with a decomposition temperature, $T_{\rm d}$, of 350 °C. Differential scanning calorimetry (DSC) analysis as shown in Figure S1 (red line) indicated a glass transition temperature (T_{σ}) of around 160 °C. TPTQ-F was soluble in common organic solvents such as toluene, p-xylene, or chlorobenzene.

As shown in Figure 1c, Figure S2, and Figure S3, the chemical modification of acceptor monomer (TPTQ vs TPTI) influenced the charge distribution, energy levels, and copolymer backbones. With carbonyl group attached to thiophen ring (from TPTI to TPTQ), the calculated LUMO energy levels were shifted downward from -1.63 eV (TPTI) to -2.18 eV (TPTQ) (B3LYP method, 6-31g** basis set), indicating a stronger electron-withdrawing capability of TPTQ (Figure S2). Both cyclic voltammetry (CV) results and the calculated LUMO and HOMO energy levels were decreased simultaneously in TPTQ-F (CV, -3.38 eV/-5.76 eV; DFT, -2.46 eV/-5.21 eV) in comparison with TPTI-F (CV, -3.15eV/-5.48 eV; DFT, -2.25 eV/-4.93 eV), as shown in Table 1 and Figure 2. The low-lying LUMO (-3.38 eV) and high-lying HOMO (-5.76 eV) energy levels in TPTQ-F thin films benefit ambipolar charge transport. Different from TPTI-F with twisted polymer backbone that impedes charge transport (Figure 1c), the enhanced planarity in TPTQ-F benefits tight and ordered molecular stacking and facilitates charge transporting.

The concentration dependent UV-vis absorption spectra of TPTQ-F were shown in Figure 3a. All the spectra in tested

Table 1. Chemical Properties of TPTQ-F

	HOMO (eV)	LUMO (eV)	$E_{\rm g}^{\ b}$ (eV)	$E_{\rm g}^{\rm film}$ (eV)	$E_{\rm g}^{\rm solution}$ (eV)	PLQY (%)	$M_{ m w}$	$M_{ m n}$	PDI	$T_{\rm d}$ (°C) ^e
TPTQ-F	-5.76^{a} -5.21^{b}	-3.38^{c} -2.46^{b}	2.75	2.38 ^d	2.45	77	55172	36012	1.53	350

"Calculated from oxidation onset of CV spectra. "Calculated from DFT. $^cE_{LUMO} = E_{HOMO} + E_g^{film}$. "Bandgap (E_g) calculated from the onset of the film absorption spectra. "TGA data showing the temperature for onset of 5% mass loss.

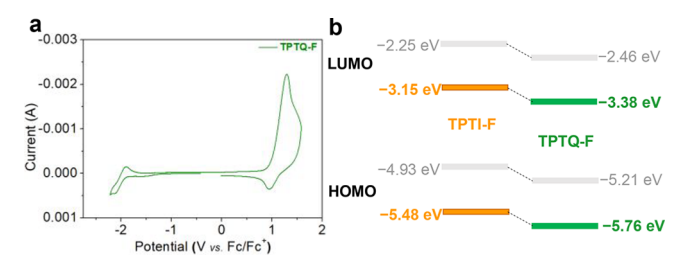


Figure 2. (a) Cyclic voltammetry (CV) curve of TPTQ-F film in acetonitrile solution (0.1 M $\mathrm{Bu_4NPF_6}$, as electrolyte) at room temperature (vs Fc/Fc⁺). (b) Energy diagram of TPTQ-F and TPTI-F, where DFT calculation results are in light gray and CV results for TPTI-F and TPTQ-F are in orange and green, respectively.

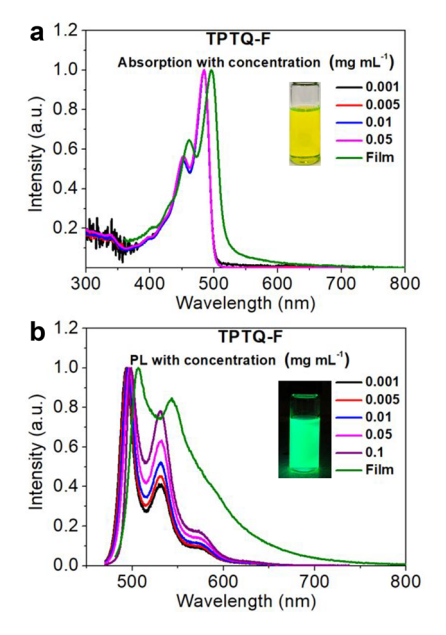


Figure 3. Concentration-dependent (mg/mL) UV—vis absorption (a) and photoluminescence (b) spectra of TPTQ-F. The insets are the optical images of TPTQ-F in CHCl₃ solution under ambient condition or UV light.

concentration range kept the same line shapes with two main sharp peaks at 452 and 484 nm, respectively. Slight red shifts to 460 and 496 nm were observed in thin films respectively. The red shifts in TPTQ-F films were expected due to increased interchain interaction in the solid state, which behaved more like the formation of J-aggregates, in contrast to H-aggregates in TPTI-F as revealed in our previous work.⁴⁷ The emission

spectrum of the TPTQ-F film exhibited two main peaks at 507 and 544 nm and a shoulder peak around 588 nm (Figure 3b), which were slightly red-shifted from that of dilute solution (494 nm, 531 nm, and 573 nm), different from excimer formed in TPTI-F films.

Although the I_{0-0}/I_{0-1} ratio decreased as concentration increased, the 0-0 transition was still the dominant emission peak. This was in contrast to that of TPTI-F, indicating the formation of J-aggregates in TPTQ-F. 39,41 To further confirm the aggregate modes in TPTQ-F, temperature dependent fluorescence spectra were performed as shown in Figure S4 and Table S2. TPTQ-F exhibited a decreased I_{0-0}/I_{0-1} ratio from 2.53 to 2.38 when the solution temperature increased from -9 to 20 °C which was consistent with J-aggregation. 39 Both thin-film absorption and fluorescent spectra of TPTQ-F behaved very similarly to that of dilute solution and showed no significant red-shift or broadening. It implied that a low degree of energetic disorder and linear conformations existed in both thin-films and solutions, which avoided strong interchain aggregates and benefited fluorescence. 45 Time-resolved fluorescence decay measurements indicated that polymer TPTQ-F exhibited the fluorescence lifetime (τ) of 0.615 ns with a single exponential decay curve (Table S3). TPTQ-F with enhanced planarity and J-aggregates showed higher PLQY (77%) than that of the analogous TPTI-F (59%), which makes this new polymer more promising in OLETs.

Single-layered thin-film OFET devices of TPTQ-F were prepared with gold (Au) as source and drain electrodes in the configuration of bottom gate top contact (BGTC) as depicted in Figure S5. After spin-coating TPTQ-F chloroform solutions on octadecyltrichlorosilane (OTS) modified silicon nitride (Si_3N_4) , the thin films were thermal-annealed (TA) at a series of temperatures from 100 to 190 °C in glovebox. As shown in Figure S5b, TPTQ-F exhibited p-channel dominant transfer curves with weak electron transport response. The hole mobilities of TPTQ-F thin films were increased with TA temperature from 100 to 120 °C and then decreased gradually to 160 °C (Figure 4a, blue line). When heating to 190 °C, the charge mobility was decreased near 2 orders of magnitude. TPTQ-F showed average hole mobility (μ_h) of 1.49 × 10⁻³ cm² V⁻¹ s⁻¹ and $I_{\text{on/off}}$ of 10⁴ at an optimized temperature of 120 °C (Table S4 and Figure S5b). These results are much improved from that of TPTI-F ($\mu_e = 1.8 \times 10^{-6} \text{ cm}^2 \text{ V}^{-1} \text{ s}^{-1}$, $I_{\rm on/off}$ of 10^1) and the other previously reported semiladder polymers 46,47 (Table 2 and Table S4). As found in atomic force microscopy (AFM) height images, the morphologies of TPTQ-F thin films were significantly changed after heating

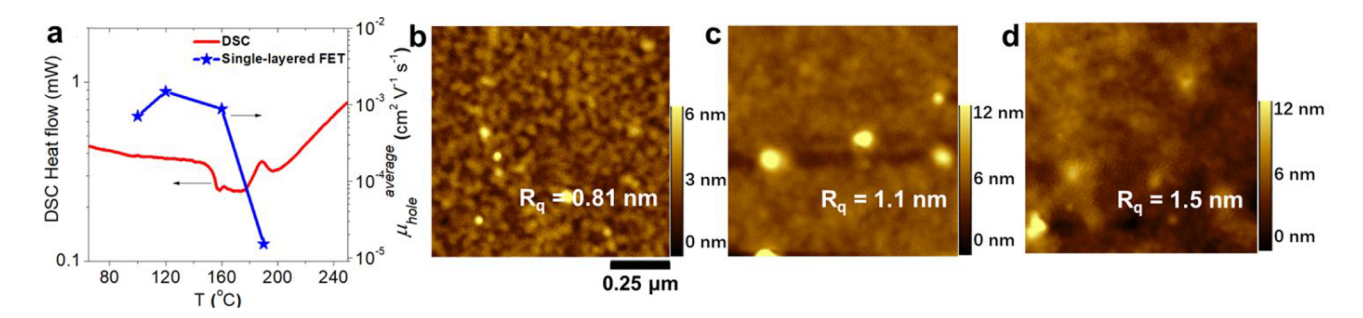


Figure 4. (a) DSC analysis (red line, the second heating scan) and average thin-film FET hole mobilities changes with thermal-annealing temperatures (blue line) for TPTQ-F. AFM images (area, $1 \times 1 \mu m^2$) of TPTQ-F thin films thermal-annealing at (b) 120 °C, (c) 160 °C, and (d) 190 °C.

Table 2. Summary of Microstructures and Electrical and Optical Properties of Semiladder Polymers Developed in Our Groups

polymer	$ \overset{d_{\pi^{-\pi}}}{(\mathrm{A})} $	scattering intensity $(\pi - \pi)$	$d_{ m Lamellar} \ ({ m \AA})$	crystallinity	aggregate modes	charge mobilities $(cm^2 V^{-1} s^{-1})^a$	PLQY (%)	ref		
TPTI-CC	3.6	17.9	21.9	amorphous	interchain J-	3.1×10^{-4}	23	47		
TPTQ-C	3.8	39.2	19.4	amorphous	intrachain H-	6.9×10^{-5}	30	46		
TPTQF-C	3.9	14.1	24.5	amorphous	intrachain H-	5.2×10^{-6}	50	46		
TPTQ-F	4.0	181	11.7	strong crystalline	interchain J-	3.0×10^{-3}	77	b		
TPTI-F	4.1	35	14.6	amorphous	interchain H- (excimer)	1.8×10^{-6}	59	47		
^a The highest value of single-layered FET's charge mobility. ^b This work.										

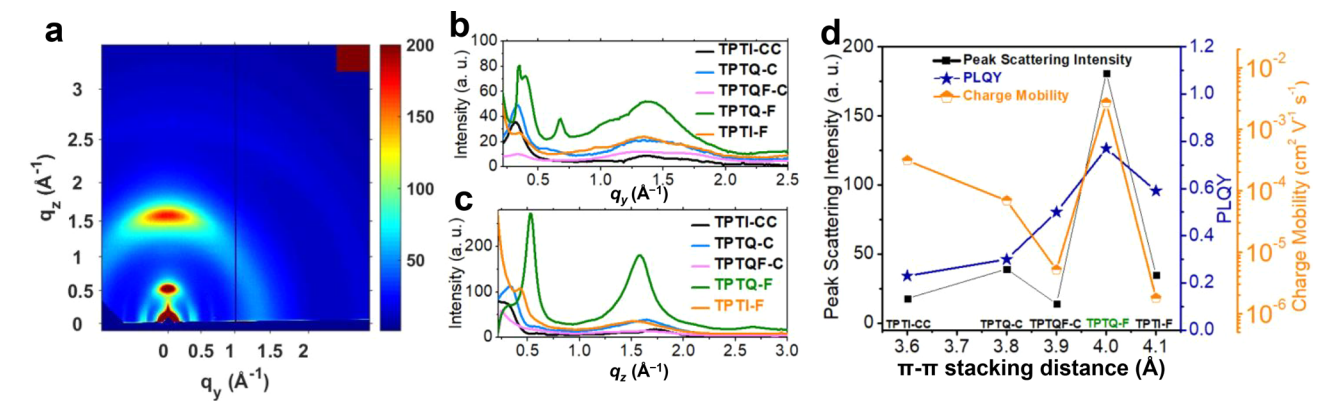


Figure 5. 2D GIWAXS image of (a) TPTQ-F with thermal-annealing temperature at 120 °C. 1D GIWAXS lineaut along in-plane (b) and out-of-plane (c) directions. (d) $\pi - \pi$ stacking scattering intensity, PLQY, and FET charge mobilities of TPTI and TPTQ based semiladder polymers change with $\pi - \pi$ stacking distance.

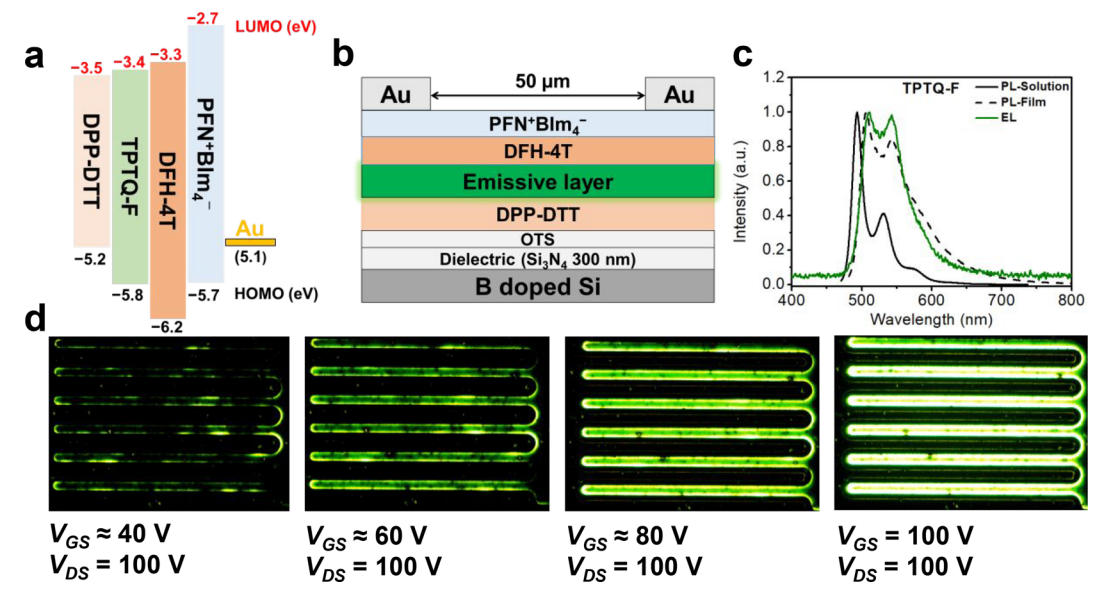


Figure 6. (a) Energy diagram of the different layers. (b) Device configuration of multilayered OLETs. (c) Photoluminescent and electroluminescent spectra of TPTQ-F. (d) EL images of TPTQ-F multilayered OLET devices with increasing gate voltages ($V_{DS} = 100 \text{ V}$). The channel length (L) of the devices is 50 μ m, and the channel width (W) is 18.2 mm.

from 120 °C (Figure 4b) to 160 °C (Figure 4c, $T_{\rm g}$ as shown in DSC analysis) and 190 °C (Figure 4d). The RMS roughness was increased from 0.81 nm to 1.1 nm and 1.5 nm with thermal annealing temperatures at 120 °C, 160 °C, and 190 °C respectively. Figure 4b exhibited uniform and continuous domain distributions, as well as highly ordered crystallinity, which was consistent with the highest charge mobility achieved at 120 °C. After heating to $T_{\rm g}$ (160 °C) and higher temperature, 190 °C, the morphologies became more disordered and nonuniform, which impeded charge transport.

To get further insight into the microstructures and explore how the intermolecular interaction influenced the charge transport and fluorescence, grazing-incidence wide-angle X-ray scattering (GIWAXS) was performed as shown in Figure 5a–c. TPTQ-F thin films showed not uniformly distributed scattering ring with more intensity in the vertical direction, and this was attributed to a typical face-on orientation. In contrast to weak crystallinity in amorphous TPTI-F, stronger scattering intensity, decreased lamellar stacking distance (11.7 Å in TPTQ-F and 14.6 Å in TPTI-F), and $\pi-\pi$ stacking

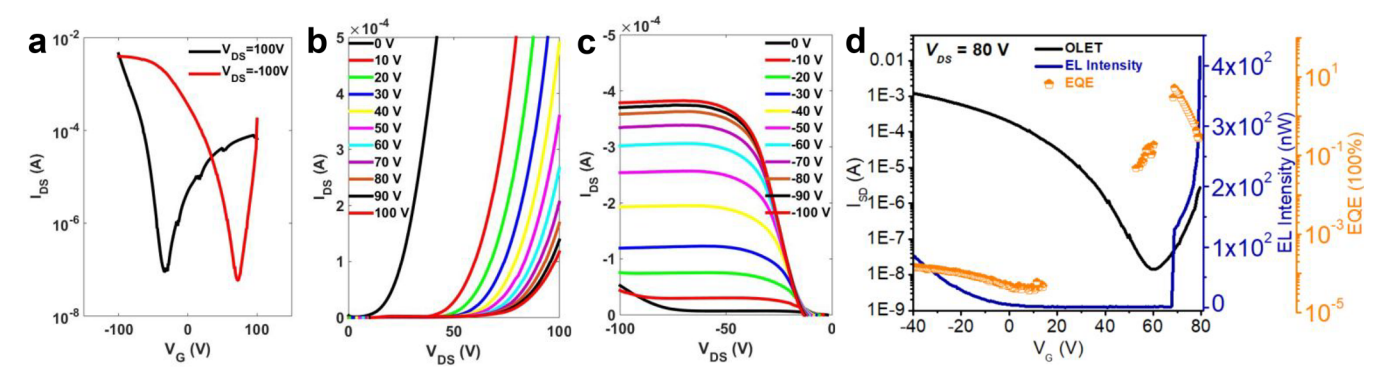


Figure 7. Multilayered OLET transfer (a) and output curves (b, c) of TPTQ-F. Source-drain current (I_{SD}), electroluminescent intensity (EL intensity), and EQE of (d) TPTQ-F changing with gate voltage ($V_{DS} = 80 \text{ V}$).

distances (4.0 Å in TPTQ-F and 4.1 Å in TPTI-F) were found in TPTQ-F thin films as shown in 1D GIWAXS linecut (Figure 5c) and Table 2. It demonstrated enhanced crystallinity and more ordered molecular stacking in TPTQ-F, which was consistent with its more planar molecular backbone and interchain J-aggregations. Interestingly, we achieved enhancement in charge carriers mobilities without sacrificing the PLQY in TPTQ-F. It was still the highest among all the semiladder polymers we developed (Figure 5d and Table 2). This can be attributed to the subtle enlargement in interchain π – π spacing (>3.9 Å) in TPTQ-F, which can retain delicate fluorescent aggregates. This is consistent with the analysis of UV–vis absorption and fluorescence spectra. 44,45

Meanwhile, it indicates that the more planar linear conjugated polymer backbone with enhanced crystallinity and decreased lamellar stacking distances in TPTQ-F plays a positive role in charge transport as shown by comparison with the other four semiladder copolymers. The high PLQY and charge mobilities achieved in TPTQ-F should make it a promising candidate in solution-processed polymer OLETs.

From the energy level diagram (Figure 6a), the LUMO energy level of TPTQ-F was aligned too high relative to work function of Au (5.1 eV) and resulted in an electron injection barrier as large as 1.7 eV, which impeded the electron transport in TPTQ-F as shown in Figure S5. With the aid of a polyelectrolyte, PFN⁺BIm₄⁻ as electron injection layer,³⁰ much balanced ambipolar transport behavior with average $\mu_{\rm h}$ of 1.26 \times 10⁻³ cm² V⁻¹ s⁻¹ and electron mobility (μ_e) of 3.53 \times 10⁻⁴ cm² V⁻¹ s⁻¹ was achieved in double layered OFET devices (Table S4 and Figure S6). Besides, $I_{\text{on/off}}$ of 10^4 and 10^3 and threshold voltages (V_T) of 14.0 V and -4.0 V were obtained in p-channel and n-channel, respectively. However, due to the moderate charge mobilities, the double-layered OFET devices of TPTQ-F showed no detectable electroluminescence in BGTC configuration with symmetric Au drain and source electrodes.

In order to simultaneously reduce the charge injection barrier and increase charge mobilities, we used multilayered OLETs ($\rm Si_3N_4/OTS/DPP\text{-}DTT/emissive\ layer/DFH\text{-}4T/PFN^+BIm_4^-/Au$) to investigate the electroluminescent properties of TPTQ-F (Figure 6b). 27,30,46 The PFN^+BIm_4^- with unique ionic effect 30 and DFH-4T 50,51 with high electron mobilities were inserted between Au and the emissive layer to decrease the electron injection barrier. The DFH-4T acted as an efficient electron transporting layer. As shown in Figure 6a, the LUMO (-3.3 eV) of DFH-4T aligned closely with the LUMO (-3.4 eV) of TPTQ-F, while HOMO (-6.3 eV) was

much deeper than that of TPTQ-F (-5.8 eV). Thus, the injection of electron from DFH-4T to TPTQ-F was accessible and DFH-4T acted as a hole blocking layer. DPP-DTT with high hole mobilities and moderate electron mobilities was inserted between the gate electrode and the emissive layer as another charge transporting layer. 52 The HOMO (-5.2 eV) and LUMO (-3.5 eV) of DPP-DTT matched well with that of the TPTQ-F, which should facilitate hole or electron transport from DPP-DTT back to the emissive layer. Notably, the device fabrication was enabled by solution-processing as shown in detail in the Supporting Information. More than 10 OLET devices were fabricated and tested for TPTQ-F. As shown in Figure 6d, yellow-green electroluminescence was observed in multilayered OLETs of TPTQ-F. The intensity of electroluminescence increased, and the emission zone became much broader and shifted away from electrodes with increased gate voltages. The EL spectrum of TPTQ-F showed two main peaks at 511 nm (0-0) and 543 nm (0-1), which were similar to those of PL spectrum of thin films (Figure 6c). The slightly decreased I_{0-0}/I_{0-1} ratio in EL spectrum can be attributed to the minor change of molecular aggregates of TPTQ-F layer in OLET devices.

The OLET output and transfer curves of TPTQ-F were shown in Figure 7, in which both positive drain-source (V_{DS}) voltages (n-channel) and negative $V_{\rm DS}$ (p-channel) exhibited ambipolar behavior with V-shape curves. It was evident that the charge transport occurred predominantly at the DPP-DTT/dielectric interface and DFH-4T/PFN⁺BIm₄⁻ interface. The calculated hole mobilities ($\mu_h = 2.58 \times 10^{-1} \text{ cm}^2 \text{ V}^{-1} \text{ s}^{-1}$) and electron mobilities ($\mu_e = 6.34 \times 10^{-3} \text{ cm}^2 \text{ V}^{-1} \text{ s}^{-1}$) from transfer curves of multilayered OLET devices were over 2 orders of magnitude and 10 times larger than for doublelayered FET devices of TPTQ-F, respectively (Table S4). The threshold voltages (V_T) were -28 and 23 V for p- and nchannel, respectively. Large on/off ratios of source-drain current $(I_{\text{on/off}})$ were obtained for both p-channel (10⁵) and n-channel (10⁴). The charge carriers' mobility in these multilayer devices were not balanced; namely, the hole mobilities were higher than that of electron, which made the recombination zone shift away from the middle (Figure 6d), in contrast to the single-layered OLETs. 53,54 The relatively low electron mobilities in OLET devices than that of OFET mobilities of pristine DFH-4T ($\mu_e = 0.5 \text{ cm}^2 \text{ V}^{-1} \text{ s}^{-1}$)^{50,51} were possibly due to the influence of highly crystallized bottom emissive layer. To measure EQE and EL intensity of the TPTQ-F OLET devices, the photon flux of OLETs devices for TPTQ-F was obtained by placing a calibrated photodiode right in front of the device and observing the response with changes of applied voltages simultaneously. S3,54 The EQE values of our OLET devices were calculated based on the photocurrent obtained from photodiodes and source-drain current in OLET devices, which can be found in detail in the Supporting Information. As shown in Figure 7d, the EL intensity decreased with decreasing gate voltages (V_G) from negative (-40 V) to positive (20 V) and then increased with increasing gate voltages starting from around $V_{\rm G}$ = 60 V. The highest EL intensity of 414 nW was achieved in OLET devices based on TPTQ-F. TPTQ-F OLET devices showed the highest EQE of 5.3% at applied voltages of $V_{\rm DS}$ = 80 V and $V_{\rm G}$ = 69 V, which was around 4 orders of magnitude higher than that of the corresponding OLED (EQE^{max} = 5.59×10^{-4} , Figure S7). Different from OLEDs, the excitons were formed relatively far away from the edge of electrodes in OLETs, which reduced the interaction between exciton and metal and minimized the quench of excitons significantly. The OLET structure avoided emitted photons passing through the highly refractive transparent indium tin oxide (ITO) electrode, resulting in higher outcoupling efficiency in OLETs. Thus, multilayered OLETs are a potentially more efficient platform for optical display than OLEDs.

CONCLUSION

A highly emissive ladder-type copolymer TPTQ-F was designed and synthesized in this work. It exhibited excellent PLQY of 77% and highly balanced ambipolar charge mobilities in double-layered OFET: $\mu_{\rm h}=1.26\times 10^{-3}~{\rm cm^2~V^{-1}~s^{-1}}$ and $\mu_{\rm e}=3.53\times 10^{-4}~{\rm cm^2~V^{-1}~s^{-1}}$. Detailed studies revealed that it was the delicate interchain $\pi-\pi$ stacking distance (4.0 Å), lower degree of energetic disordered, and enhanced crystallinity that contributed to the impressive fluorescence and charge transport. Moreover, the multilayered OLET devices based on TPTQ-F showed an EQE as high as 5.3% and an electroluminescent intensity of 414 nW. This work also indicates that the multilayered OLET structure with matched energy levels and good charge transporting layer is crucial when the emissive layer exhibits only moderate carrier's mobility.

ASSOCIATED CONTENT

Supporting Information

The Supporting Information is available free of charge at https://pubs.acs.org/doi/10.1021/jacs.1c01659.

Fabrication and characterization of FETs, OLEDs, and OLETs; temperature-dependent PL spectra; DFT calculation results of monomers and copolymers (PDF)

AUTHOR INFORMATION

Corresponding Author

Luping Yu — Department of Chemistry and the James Franck Institute, The University of Chicago, Chicago, Illinois 60637, United States; Email: lupingyu@uchicago.edu

Authors

Dafei Yuan — Department of Chemistry and the James Franck Institute, The University of Chicago, Chicago, Illinois 60637, United States; o orcid.org/0000-0001-5914-2060

- Mohammad A. Awais Department of Chemistry and the James Franck Institute, The University of Chicago, Chicago, Illinois 60637, United States
- Valerii Sharapov Department of Chemistry and the James Franck Institute, The University of Chicago, Chicago, Illinois 60637, United States
- Xunshan Liu Department of Chemistry and the James Franck Institute, The University of Chicago, Chicago, Illinois 60637, United States; orcid.org/0000-0003-1537-258X
- Andriy Neshchadin Department of Chemistry and the James Franck Institute, The University of Chicago, Chicago, Illinois 60637, United States; orcid.org/0000-0002-8548-1186
- Wei Chen Materials Science Division and Center for Molecular Engineering, Argonne National Laboratory, Lemont, Illinois 60439, United States; orcid.org/0000-0001-8906-4278

Complete contact information is available at: https://pubs.acs.org/10.1021/jacs.1c01659

Notes

The authors declare no competing financial interest.

ACKNOWLEDGMENTS

This work was supported by NSF (Grant Chem-1802274, L.Y.), partially supported by the University of Chicago Materials Research Science and Engineering Center, which is funded by the National Science Foundation under Award DMR-1420709. We also thank Dr. Joseph Strzalka and Dr. Zhang Jiang for the assistance with GIWAXS measurements. This research used resources of the Advanced Photon Source, a U.S. Department of Energy (DOE) Office of Science User Facility operated for the DOE Office of Science by Argonne National Laboratory under Contract DE-AC02-06CH11357.

REFERENCES

- (1) Heeger, A. J. Semiconducting and Metallic Polymers: The Fourth Generation of Polymeric Materials (Nobel Lecture). *Angew. Chem., Int. Ed.* **2001**, *40*, 2591–2611.
- (2) Ostroverkhova, O. Organic Optoelectronic Materials: Mechanisms and Applications. *Chem. Rev.* **2016**, *116*, 13279–13412.
- (3) Meng, L.; Zhang, Y.; Wan, X.; Li, C.; Zhang, X.; Wang, Y.; Ke, X.; Xiao, Z.; Ding, L.; Xia, R.; Yip, H. L.; Cao, Y.; Chen, Y. Organic and Solution-Processed Tandem Solar Cells with 17.3% Efficiency. *Science* 2018, 361, 1094–1098.
- (4) Chen, H.; Zhang, W.; Li, M.; He, G.; Guo, X. Interface Engineering in Organic Field-Effect Transistors: Principles, Applications, and Perspectives. *Chem. Rev.* **2020**, *120*, 2879–2949.
- (5) Mei, J.; Diao, Y.; Appleton, A. L.; Fang, L.; Bao, Z. Integrated Materials Design of Organic Semiconductors for Field-Effect Transistors. *J. Am. Chem. Soc.* **2013**, *135*, 6724–46.
- (6) Wong, M. Y.; Zysman-Colman, E. Purely Organic Thermally Activated Delayed Fluorescence Materials for Organic Light-Emitting Diodes. *Adv. Mater.* **2017**, *29*, 1605444.
- (7) Zhang, D.; Huang, T.; Duan, L. Emerging Self-Emissive Technologies for Flexible Displays. *Adv. Mater.* **2020**, 32, 1902391.
- (8) Hepp, A.; Heil, H.; Weise, W.; Ahles, M.; Schmechel, R.; von Seggern, H. Light-Emitting Field-Effect Transistor Based on a Tetracene Thin Film. *Phys. Rev. Lett.* **2003**, *91*, 157406.
- (9) Zhang, C.; Chen, P.; Hu, W. Organic Light-Emitting Transistors: Materials, Device Configurations, and Operations. *Small* **2016**, *12*, 1252–94
- (10) Liu, C. F.; Liu, X.; Lai, W. Y.; Huang, W. Organic Light-Emitting Field-Effect Transistors: Device Geometries and Fabrication Techniques. *Adv. Mater.* **2018**, *30*, 1802466.

- (11) Zaumseil, J. Recent Developments and Novel Applications of Thin Film, Light-Emitting Transistors. *Adv. Funct. Mater.* **2020**, *30*, 1905269.
- (12) Yuan, D.; Sharapov, V.; Liu, X.; Yu, L. Design of High-Performance Organic Light-Emitting Transistors. *ACS Omega* **2020**, *5*, 68–74.
- (13) Kahmann, S.; Shulga, A.; Loi, M. A. Quantum Dot Light-Emitting Transistors—Powerful Research Tools and Their Future Applications. *Adv. Funct. Mater.* **2020**, *30*, 1904174.
- (14) Bisri, S. Z.; Piliego, C.; Gao, J.; Loi, M. A. Outlook and Emerging Semiconducting Materials for Ambipolar Transistors. *Adv. Mater.* **2014**, 26, 1176–99.
- (15) Baronas, P.; Kreiza, G.; Mamada, M.; Maedera, S.; Adomėnas, P.; Adomėnienė, O.; Kazlauskas, K.; Adachi, C.; Juršėnas, S. Enhanced Energy Transfer in Doped Bifluorene Single Crystals: Prospects for Organic. *Adv. Opt. Mater.* **2020**, *8*, 1901670.
- (16) Sandanayaka, A. S. D.; Matsushima, T.; Bencheikh, F.; Terakawa, S.; Potscavage, W. J.; Qin, C.; Fujihara, T.; Goushi, K.; Ribierre, J.-C.; Adachi, C. Indication of Current-Injection Lasing from an Organic Semiconductor. *Appl. Phys. Express* **2019**, *12*, 061010.
- (17) Han, Y.; Bai, L.; Xu, M.; An, X.; Wei, C.; Sun, L.; Sun, N.; Yu, M.; Zhang, H.; Lin, J.; Ou, C.; Xie, L.; Yin, C.; Sun, C.; Ding, X.; Cabanillas-Gonzalez, J.; Huang, W. Deep-Blue Thiophene-Based Steric Oligomers as a Low-Threshold Laser Gain and Host Material. *Adv. Opt. Mater.* **2020**, *8*, 1902163.
- (18) Jiang, Y.; Liu, Y. Y.; Liu, X.; Lin, H.; Gao, K.; Lai, W. Y.; Huang, W. Organic Solid-State Lasers: A Materials View and Future Development. *Chem. Soc. Rev.* **2020**, *49*, 5885–5944.
- (19) Liu, D.; De, J.; Gao, H.; Ma, S.; Ou, Q.; Li, S.; Qin, Z.; Dong, H.; Liao, Q.; Xu, B.; Peng, Q.; Shuai, Z.; Tian, W.; Fu, H.; Zhang, X.; Zhen, Y.; Hu, W. Organic Laser Molecule with High Mobility, High Photoluminescence Quantum Yield, and Deep-Blue Lasing Characteristics. J. Am. Chem. Soc. 2020, 142, 6332–6339.
- (20) Toffanin, S.; Capelli, R.; Koopman, W.; Generali, G.; Cavallini, S.; Stefani, A.; Saguatti, D.; Ruani, G.; Muccini, M. Organic Light-Emitting Transistors with Voltage-Tunable Lit Area and Full Channel Illumination. *Laser & Photonics Reviews* **2013**, *7*, 1011–1019.
- (21) Muccini, M.; Koopman, W.; Toffanin, S. The Photonic Perspective of Organic Light-Emitting Transistors. *Laser & Photonics Reviews* **2012**, *6*, 258–275.
- (22) Qin, Z.; Gao, H.; Liu, J.; Zhou, K.; Li, J.; Dang, Y.; Huang, L.; Deng, H.; Zhang, X.; Dong, H.; Hu, W. High-Efficiency Single-Component Organic Light-Emitting Transistors. *Adv. Mater.* **2019**, *31*, 1903175.
- (23) Park, S. K.; Kim, J. H.; Ohto, T.; Yamada, R.; Jones, A. O. F.; Whang, D. R.; Cho, I.; Oh, S.; Hong, S. H.; Kwon, J. E.; Kim, J. H.; Olivier, Y.; Fischer, R.; Resel, R.; Gierschner, J.; Tada, H.; Park, S. Y. Highly Luminescent 2d-Type Slab Crystals Based on a Molecular Charge-Transfer Complex as Promising Organic Light-Emitting Transistor Materials. *Adv. Mater.* 2017, 29, 1701346.
- (24) Zheng, L.; Li, J.; Zhou, K.; Yu, X.; Zhang, X.; Dong, H.; Hu, W. Molecular-Scale Integrated Multi-Functions for Organic Light-Emitting Transistors. *Nano Res.* **2020**, *13*, 1976–1981.
- (25) Hu, Y.; Song, L.; Zhang, S.; Lv, Y.; Lin, J.; Guo, X.; Liu, X. Improving the Efficiency of Multilayer Organic Light-Emitting Transistors by Exploring the Hole Blocking Effect. *Adv. Mater. Interfaces* **2020**, *7*, 2000657.
- (26) Chen, H.; Xing, X.; Miao, J.; Zhao, C.; Zhu, M.; Bai, J.; He, Y.; Meng, H. Highly Efficient Flexible Organic Light Emitting Transistor Based on High-K Polymer Gate Dielectric. *Adv. Opt. Mater.* **2020**, *8*, 1901651.
- (27) Capelli, R.; Toffanin, S.; Generali, G.; Usta, H.; Facchetti, A.; Muccini, M. Organic Light-Emitting Transistors with an Efficiency That Outperforms the Equivalent Light-Emitting Diodes. *Nat. Mater.* **2010**, *9*, 496–503.
- (28) Wan, Y.; Deng, J.; Wu, W.; Zhou, J.; Niu, Q.; Li, H.; Yu, H.; Gu, C.; Ma, Y. Efficient Organic Light-Emitting Transistors Based on High-Quality Ambipolar Single Crystals. *ACS Appl. Mater. Interfaces* **2020**, *12*, 43976–43983.

- (29) Liu, Y.; Guo, Y.; Liu, Y. High-Mobility Organic Light-Emitting Semiconductors and Its Optoelectronic Devices. *Small Struct.* **2021**, *2*, 2000083.
- (30) Seo, J. H.; Namdas, E. B.; Gutacker, A.; Heeger, A. J.; Bazan, G. C. Solution-Processed Organic Light-Emitting Transistors Incorporating Conjugated Polyelectrolytes. *Adv. Funct. Mater.* **2011**, *21*, 3667–3672.
- (31) Roelofs, W. S. C.; Adriaans, W. H.; Janssen, R. A. J.; Kemerink, M.; de Leeuw, D. M. Light Emission in the Unipolar Regime of Ambipolar Organic Field-Effect Transistors. *Adv. Funct. Mater.* **2013**, 23, 4133–4139.
- (32) Ullah, M.; Tandy, K.; Yambem, S. D.; Aljada, M.; Burn, P. L.; Meredith, P.; Namdas, E. B. Simultaneous Enhancement of Brightness, Efficiency, and Switching in Rgb Organic Light Emitting Transistors. *Adv. Mater.* **2013**, *25*, 6213–8.
- (33) Ullah, M.; Armin, A.; Tandy, K.; Yambem, S. D.; Burn, P. L.; Meredith, P.; Namdas, E. B. Defining the Light Emitting Area for Displays in the Unipolar Regime of Highly Efficient Light Emitting Transistors. *Sci. Rep.* **2015**, *5*, 8818.
- (34) Ullah, M.; Tandy, K.; Li, J.; Shi, Z.; Burn, P. L.; Meredith, P.; Namdas, E. B. High-Mobility, Heterostructure Light-Emitting Transistors and Complementary Inverters. *ACS Photonics* **2014**, *1*, 954–959.
- (35) Li, J.; Zhou, K.; Liu, J.; Zhen, Y.; Liu, L.; Zhang, J.; Dong, H.; Zhang, X.; Jiang, L.; Hu, W. Aromatic Extension at 2,6-Positions of Anthracene toward an Elegant Strategy for Organic Semiconductors with Efficient Charge Transport and Strong Solid State Emission. *J. Am. Chem. Soc.* 2017, 139, 17261–17264.
- (36) Zhang, X.; Dong, H.; Hu, W. Organic Semiconductor Single Crystals for Electronics and Photonics. *Adv. Mater.* **2018**, *30*, 1801048.
- (37) Dadvand, A.; Moiseev, A. G.; Sawabe, K.; Sun, W. H.; Djukic, B.; Chung, I.; Takenobu, T.; Rosei, F.; Perepichka, D. F. Maximizing Field-Effect Mobility and Solid-State Luminescence in Organic Semiconductors. *Angew. Chem., Int. Ed.* **2012**, *51*, 3837–41.
- (38) Liu, J.; Zhang, H.; Dong, H.; Meng, L.; Jiang, L.; Jiang, L.; Wang, Y.; Yu, J.; Sun, Y.; Hu, W.; Heeger, A. J. High Mobility Emissive Organic Semiconductor. *Nat. Commun.* **2015**, *6*, 10032.
- (39) Spano, F. C.; Silva, C. H- and J-Aggregate Behavior in Polymeric Semiconductors. *Annu. Rev. Phys. Chem.* **2014**, *65*, 477–500
- (40) Deng, Y.; Yuan, W.; Jia, Z.; Liu, G. H- and J-Aggregation of Fluorene-Based Chromophores. *J. Phys. Chem. B* **2014**, *118*, 14536–45.
- (41) Spano, F. C. The Spectral Signatures of Frenkel Polarons in H-and J-Aggregates. *Acc. Chem. Res.* **2010**, *43*, 429–39.
- (42) Zheng, C.; Zhong, C.; Collison, C. J.; Spano, F. C. Non-Kasha Behavior in Quadrupolar Dye Aggregates: The Red-Shifted H-Aggregate. *J. Phys. Chem. C* **2019**, *123*, 3203–3215.
- (43) Donley, C. L.; Zaumseil, J.; Andreasen, J. W.; Nielsen, M. M.; Sirringhaus, H.; Friend, R. H.; Kim, J. S. Effects of Packing Structure on the Optoelectronic and Charge Transport Properties in Poly(9,9-Di-N-Octylfluorene-Alt-Benzothiadiazole). *J. Am. Chem. Soc.* **2005**, 127, 12890–9.
- (44) McQuade, D. T.; Kim, J.; Swager, T. M. Two-Dimensional Conjugated Polymer Assemblies: Interchain Spacing for Control of Photophysics. *J. Am. Chem. Soc.* **2000**, *122*, 5885–5886.
- (45) Leventis, A.; Royakkers, J.; Rapidis, A. G.; Goodeal, N.; Corpinot, M. K.; Frost, J. M.; Bucar, D. K.; Blunt, M. O.; Cacialli, F.; Bronstein, H. Highly Luminescent Encapsulated Narrow Bandgap Polymers Based on Diketopyrrolopyrrole. *J. Am. Chem. Soc.* **2018**, 140, 1622–1626.
- (46) Yuan, D.; Awais, M. A.; Sharapov, V.; Liu, X.; Neshchadin, A.; Chen, W.; Bera, M.; Yu, L. Foldable Semi-Ladder Polymers: Novel Aggregation Behavior and High-Performance Solution-Processed Organic Light-Emitting Transistors. *Chem. Sci.* **2020**, *11*, 11315—11321
- (47) Yuan, D.; Awais, M. A.; Sharapov, V.; Liu, X.; Neshchadin, A.; Chen, W.; Yu, L. Highly Emissive Semi-Ladder-Type Copolymers,

- Aggregation State, and Solution-Processed Organic Light-Emitting Transistor. Chem. Mater. 2020, 32, 4672–4680.
- (48) Jung, I. H.; Lo, W.-Y.; Jang, J.; Chen, W.; Zhao, D.; Landry, E. S.; Lu, L.; Talapin, D. V.; Yu, L. Synthesis and Search for Design Principles of New Electron Accepting Polymers for All-Polymer Solar Cells. *Chem. Mater.* **2014**, *26*, 3450–3459.
- (49) Jung, I. H.; Zhao, D.; Jang, J.; Chen, W.; Landry, E. S.; Lu, L.; Talapin, D. V.; Yu, L. Development and Structure/Property Relationship of New Electron Accepting Polymers Based on Thieno[2',3':4,5]Pyrido[2,3-G]Thieno[3,2-C]Quinoline-4,10-Dione for All-Polymer Solar Cells. *Chem. Mater.* **2015**, *27*, 5941–5948.
- (50) Facchetti, A.; Mushrush, M.; Yoon, M.-H.; Hutchison, G. R.; Ratner, M. A.; Marks, T. J. Building Blocks for N-Type Molecular and Polymeric Electronics. Perfluoroalkyl- Versus Alkyl-Functionalized Oligothiophenes (Nt;N= 2–6). Systematics of Thin Film Microstructure, Semiconductor Performance, and Modeling of Majority Charge Injection in Field-Effect Transistors. J. Am. Chem. Soc. 2004, 126, 13859–13874.
- (51) Usta, H.; Facchetti, A.; Marks, T. J. N-Channel Semiconductor Materials Design for Organic Complementary Circuits. *Acc. Chem. Res.* **2011**, *44*, 501–10.
- (52) Li, J.; Zhao, Y.; Tan, H. S.; Guo, Y.; Di, C. A.; Yu, G.; Liu, Y.; Lin, M.; Lim, S. H.; Zhou, Y.; Su, H.; Ong, B. S. A Stable Solution-Processed Polymer Semiconductor with Record High-Mobility for Printed Transistors. *Sci. Rep.* **2012**, *2*, 754.
- (53) Zaumseil, J.; Donley, C. L.; Kim, J. S.; Friend, R. H.; Sirringhaus, H. Efficient Top-Gate, Ambipolar, Light-Emitting Field-Effect Transistors Based on a Green-Light-Emitting Polyfluorene. *Adv. Mater.* **2006**, *18*, 2708–2712.
- (54) Gwinner, M. C.; Kabra, D.; Roberts, M.; Brenner, T. J.; Wallikewitz, B. H.; McNeill, C. R.; Friend, R. H.; Sirringhaus, H. Highly Efficient Single-Layer Polymer Ambipolar Light-Emitting Field-Effect Transistors. *Adv. Mater.* **2012**, *24*, 2728–34.